Nanoscale Advances

ROYAL SOCIETY OF CHEMISTRY

PAPER

View Article Online
View Journal | View Issue

Check for updates

Cite this: *Nanoscale Adv.*, 2026, **8**, 207

Preparation and evaluation of lactoferrin-modified curcumin long-circulating nanoliposomes for hypoxic brain injury therapy

Yu Xue,[a] Jinjie Liu,[b] Faisal Raza,[c] Hajra Zafar,[c] Hong Zhao,[d] Ran Li[e] and Zanhua Liu *[f]

Nanoformulations of curcumin (Cur) are advanced but still have shortcomings in terms of fast *in vivo* elimination, inefficient delivery and biodistribution of drugs to target sites. Herein, Cur liposomes (Cur-L), Cur long-circulating liposomes (Cur-LCL), and lactoferrin (Lf)-modified Cur long-circulating liposomes (Lf-Cur-LCL) were prepared using ethanol injection before application in hypoxic brain injury. Hematoxylin-eosin (HE)-stained pathological sections of the brain, liver, and spleen were examined to assess the extent of tissue damage and efficacy of treatments. Additionally, immunohistochemical staining of brain tissue was performed to assess the expression of key biomarkers involved in apoptosis. The prepared Cur-L, Cur-LCL and Lf-Cur-LCL displayed smaller particle sizes, good polymer-dispersity index, and stability over one week. The *in vitro* release behavior of Cur-L, Cur-LCL, and Lf-Cur-LCL was significantly better than that of Cur, with Cur-LCL and Lf-Cur-LCL showing better sustained release effects. Also, Cur-L, Cur-LCL, and Lf-Cur-LCL significantly prolonged the retention time of Cur *in vivo* with Lf-Cur-LCL significantly increasing Cur content in brain tissues. Furthermore, Cur-L, Cur-LCL, and Lf-Cur-LCL increased the partial pressure of oxygen and decreased the partial pressure of carbon dioxide in chronic intermittent hypoxia model mice. These formulations also elevated levels of superoxide dismutase and reduced malondialdehyde levels in the model group. Furthermore, they also demonstrated a reparative effect on liver, brain, and spleen damage induced by the model, with Lf-Cur-LCL showing the most significant therapeutic effect. In conclusion, the prepared Lf-Cur-LCL exhibited brain-targeting properties and showed considerable potential for treating brain diseases, thus providing theoretical support for clinical development and application of curcumin.

Received 28th May 2025
Accepted 6th November 2025

DOI: 10.1039/d5na00521c

rsc.li/nanoscale-advances

Open Access Article. Published on 07 November 2025. Downloaded on 1/9/2026 2:42:34 PM.
This article is licensed under a Creative Commons Attribution-NonCommercial 3.0 Unported Licence.

1 Introduction

Obstructive sleep apnea-hypopnea syndrome (OSAHS) is a common chronic condition in otorhinolaryngology[1] with roughly one billion individuals affected globally.[2,3] Its primary pathophysiological mechanism is chronic intermittent hypoxia (CIH), which is characterized by partial or complete collapse of the upper airway during sleep, leading to reduced oxygen levels, apneic events, or hypopnea.[4] This results in transient airway reopening, followed by hyperventilation and normalization of blood oxygen saturation, but the individual can experience repeated airway obstruction and hypoxia upon reentry into sleep. This cyclical hypoxia-reoxygenation process resembles the ischemia-reperfusion injury mechanism and significantly impacts human health.[5]

OSA is an independent risk factor for numerous diseases, particularly those that affect the cardiovascular system.[6] The main pathological change in OSA involves a cytokine response, with research indicating that OSA-associated chronic hypoxia activates reactive oxygen species (ROS), triggering pathways like nuclear factor-kappa B (NF-κB) and hypoxia inducible factor 1-alpha (HIF-1α), which can induce various diseases.[7] In particular, Diaz and colleagues discovered a strong association between severity of OSA and activation of NOD-like receptor protein 3 (NLRP3) with concomitant release of tissue factors, interleukin (IL)-1 beta and IL-18.[8] In terms of posing health risks, OSA has been found to cause damage to the brain and lung tissues.

Current clinical approaches include weight loss, smoking cessation, positional therapy, and surgical interventions. As the standard treatment strategy for OSA, continuous positive airway

[a]*Department of Clinical Stage 1 Experimental Ward, Shanghai Pudong new area People's Hospital, Shanghai 201299, China. E-mail: Xueyu@shpdph.com*
[b]*Department of General Practice Ward, Central Hospital of Dalian University of Technology (Dalian Municipal Central Hospital), Dalian 116033, Liaoning, China*
[c]*School of Pharmacy, Shanghai Jiao Tong University, Shanghai 200240, China*
[d]*Department of Neurology, Central Hospital of Dalian University of Technology (Dalian Municipal Central Hospital), Dalian 116033, Liaoning, China*
[e]*Department of Pharmaceutics, School of Pharmacy, Jiangsu University, Zhenjiang 212016, Jiangsu, China*
[f]*Department of Neurology, Shanghai Pudong new area People's Hospital, Shanghai 201299, China. E-mail: liuzanhua@shpdph.com*

© 2026 The Author(s). Published by the Royal Society of Chemistry

Open Access Article. Published on 07 November 2025. Downloaded on 1/9/2026 2:42:34 PM.
This article is licensed under a Creative Commons Attribution-NonCommercial 3.0 Unported Licence.

pressure (CPAP) is considered for potential reduction of oxidative stress and inflammation in OSA individuals.[9] However, CPAP is limited by inability to completely relieve OSA patients from recurrent hypoxic induced systemic inflammation and oxidative stress.[9] In an attempt to address this challenge, recent research has focused on identifying therapeutic agents from natural products, especially those that can modulate the pathways of inflammation and attenuate oxidative stress. Recent systematic review has revealed the potential of Chinese herbal medicine to improve symptoms of OSA and its comorbidities.[10] More specifically, Badria and colleagues suggested that lignans, isoflavones and cinnamic acid derivatives demonstrated the potential to effectively manage OSA.[11]

Curcumin (Cur), a polyphenolic compound is extracted from turmeric rhizomes, and has been found to exhibit anti-inflammatory, antioxidant, and anti-tumor activities.[7] It has shown potential in correcting metabolic disorders, providing neuroprotection, and alleviating depression.[12] In high-altitude regions, the harmful effects of low pressure and hypoxia on OSA necessitate the exploration of effective protective measures. Recent studies suggest that Cur has significant clinical potential in this context.[13] For example, Moulin and colleagues discovered that Cur could prevent myocardial injury induced by CIH,[14] which is a distinctive characteristic of OSA. Besides, Wang and co-workers showed that Cur demonstrated neuroprotective effects by ameliorating brain injury that was induced by CIH-related OSA through regulation of AQP4 by the p38-mitogen-activated protein kinase (MAPK) pathway.[15] Furthermore, Cur could prevent structural changes in and loss of neurons in the chronic sleep deprivation rat model.[16] The findings of these studies suggest that Cur may potentially treat OSA through mitigation of inflammation and oxidative stress.

Despite the extensive research on Cur, a critical gap remains in the development of formulations designed for brain-targeted therapies, particularly in overcoming the blood–brain barrier (BBB). While various Cur formulations, such as nanoemulsions and liposomes, have been developed to improve bioavailability of the polyphenol, they still face significant limitations in effectively delivering Cur to the brain. The primary challenge is Cur's inherent low solubility, which not only reduces its bioavailability but also hinders its ability to cross the BBB efficiently. As a result, even advanced formulations have struggled to achieve therapeutic levels of Cur in brain tissues. This limitation remains a major barrier to utilizing Cur for treating brain-related disorders such as OSA-induced brain injury. Therefore, there is a pressing need for more effective drug delivery systems capable of facilitating Cur's passage through the BBB and ensuring it reaches therapeutic concentrations in the brain.

To address these limitations, our research focused on developing Lf-Cur-LCL that could enhance Cur's ability to cross the BBB and target the brain. Although various nano-formulations of Cur, including nanoemulsions,[17] liposome nanoparticles,[18] solid lipid dispersions,[19] nanoconjugates,[20] carbon dots,[21] nanofibers,[22] hydrogels,[23] carbon nanotubes,[24] cyclodextrin-based nanocarriers, marinosomes long-circulating liposomes[25–27] and polymeric micelles[28] have been explored, they still lack effective applications for treating OSA-induced brain injury. While these formulations have been used for various purposes, they continue to face issues such as rapid *in vivo* elimination, inefficient drug delivery, and poor biodistribution to target sites. More critically for the treatment of brain injuries, most of these systems lack an active targeting mechanism to efficiently cross the intact BBB. Therefore, the proposed Lf-Cur-LCL formulation represents a significant step forward, offering a promising solution for improving Cur delivery to the brain and providing potential therapeutic effects for OSA-induced brain injury. Liposomal formulations are a widely investigated drug delivery system, prized for their ability to encapsulate both hydrophilic and hydrophobic drugs, such as Cur, thereby enhancing solubility and stability.[29] Conventional liposomes, however, are rapidly recognized and cleared by the reticuloendothelial system (RES), primarily in the liver and spleen, which drastically limits their circulation time and therapeutic potential.[30] The emergence of "nanoliposomes" represents a significant advancement to overcome this limitation. While all liposomes are by definition colloidal particles, the term "nanoliposome" specifically emphasizes vesicles that are engineered at the nanoscale. A cornerstone of their design is the precise control over particle size (PS). For systemic administration and effective passive targeting to diseased sites (*e.g.*, tumors or inflamed tissues), the optimal PS is widely acknowledged to fall within the range of approximately 100 to 200 nanometers.[31] This critical size range enables nanoliposomes to evade rapid clearance by the RES, thereby achieving a prolonged circulation half-life, while also facilitating their extravasation and accumulation through the enhanced permeability and retention (EPR) effect.[32]

A key strategy to further enhance circulation and introduce targeting capability involves surface functionalization, such as coating with hydrophilic polymers like polyethylene glycol (PEG) to create "stealth" long-circulating nanoliposomes.[33] However, long-circulating liposomes have a challenge regarding their inability to enter the brain *via* crossing of the BBB.[34] Available studies have indicated that PEGylated liposomes were able to cross the BBB through an EPR effect only when the barrier was opened *via* traumatic brain injury. The BBB is a complex, multidimensional barrier system comprising brain microvascular endothelial cells, pericytes, astrocytes, and various neurons. It isolates the central nervous system from systemic circulation, preventing toxin and pathogen entry while limiting therapeutic molecule absorption. Many biological BBBs express Lf receptors, facilitating unidirectional Lf-mediated transcytosis into the brain.[35] Based on this reason, surface functionalized PEGylated liposomes have been modified with ligands to cross the BBB. As a multifunctional glycoprotein, Lf has been used to modify the surface of various nanoparticles, because within the endothelial cells of brain capillaries, it can cross the BBB *via* transcytosis processes.[36] Its well-documented roles as a natural therapeutic agent, drug nanocarrier, and targeting ligand further establish it as an ideal candidate for brain-targeted delivery systems.[37] The Lf-modified PEGylated liposomes have been used for various applications.[38] For instance, studies have consistently demonstrated the

 © 2026 The Author(s). Published by the Royal Society of Chemistry

Open Access Article. Published on 07 November 2025. Downloaded on 1/9/2026 2:42:34 PM.
This article is licensed under a Creative Commons Attribution-NonCommercial 3.0 Unported Licence.

technical feasibility of fabricating Lf-modified (PEGylated) liposomes, confirming their stability and efficacy in cellular uptake and targeted drug delivery.[39] De Luca and colleagues developed long-circulating liposomes and modified their surfaces with Lf and antitransferrin, wherein the liposomes enhanced targeting of senktide (a peptide) to the brain.[40] Also, Wu and co-workers prepared transferrin-modified etomidate-loaded liposomes which increased the general anesthetic effect of the drug through increased brain targeting.[41] Besides, Yang and co-experimenters fabricated Ce/Zr-MOF@Cur-Lf nanoparticles that increased delivery of the polyphenol across the BBB and targeted the brain.[42] This study therefore aims to develop Lf-Cur-LCL that synergistically address the key limitations of Cur, namely its inherent poor solubility, the rapid systemic clearance of conventional formulations, and most importantly, the lack of efficient brain-targeting capabilities. We hypothesize that this integrated strategy will significantly enhance the delivery and therapeutic efficacy of Cur for the treatment of cerebral injuries induced by CIH.

2 Materials and methods

2.1 Materials and reagents

Cur, desmethoxycurcumin (DMC, internal standard IS), 1-(3-dimethylaminopropyl)-3-ethylcarbodiimide (EDC) and *N*-hydroxysuccinimide (NHS) were purchased from Shanghai Macklin Biochemical Co., Ltd. Soybean lecithin, cholesterol, PEG_{2000}-DSPE + PEG_{2000}-DSPE-COOH, dialysis bags and Sephadex G-50 were obtained from Shanghai Yuanye Bio-Technology Co., Ltd. Phosphoric acid was purchased from Titan Technology Co., Ltd. (Shanghai). Diethyl ether, ethanol, methanol, acetic acid, acetonitrile, and hydrochloric acid were obtained from Sinopharm Chemical Reagent Co., Ltd. Ethyl carbamate was purchased from Sigma-Aldrich. DMEM/F12 medium was provided by Thermo Fisher Scientific. Shanghai Yimiao Chemical Technology Co., Ltd supplied 1% Triton X-100. The HE staining kit was purchased from Beijing Solarbio Science and Technology Co., Ltd. Superoxide dismutase (SOD) and malondialdehyde (MDA) assay kits were obtained from Shanghai Yubo Biotechnology Co., Ltd.

Regarding the experimental animals that were used for this study, Sprague Dawley (SD) rats (male, 200 ± 10 g) and C57BL/6 male mice (20 ± 2 g) were supplied by the Jiangsu University Institute for Animal Care and Use Committee. The same committee approved the protocol (Approval number: UJS-IACUC-2023052402) of this study, which was performed in accordance with the National Research Council Guide for the Care and Use of Laboratory Animals.

2.2 Preparation of Lf-modified Cur-LCL

Liposomes were prepared using the ethanol injection method.[43] Cur (18.0 mg), soybean lecithin (180.0 mg), cholesterol (18.0 mg), and PEG_{2000}-DSPE + PEG_{2000}-DSPE-COOH (8.0 mg + 2.0 mg) were accurately weighed and dissolved in 5.0 mL of ethanol, which acted as the organic phase. Phosphate buffer solution (PBS, pH 6.5) was used as the aqueous phase. Under a stirring speed of 1200 revolutions minute^{-1}, the organic phase was uniformly and slowly dropped into the aqueous phase and maintained at 50 °C. Afterward, the mixture was continuously stirred for 2 hours to evaporate the organic solvent to obtain Cur-LCL. Using the same method, but without addition of PEG_{2000}-DSPE + PEG_{2000}-DSPE-COOH, we prepared conventional Cur liposomes (Cur-L) for comparison.

1-ethyl-3-(3-dimethyl-aminopropyl)-carbodiimide (EDC) and *N*-hydroxysuccinimide (NHS) (EDC: NHS: DSPE-PEG-COOH = 10 : 10 : 1, mol mol^{-1} mol^{-1}) were added to the Cur-LCL and stirred at room temperature for 10 minutes. Afterward, Lf (Lf: DSPE-PEG-COOH = 1 : 4, mol mol^{-1}) was added and incubated in a 37 °C water bath for 3 hours. Unreacted EDC, NHS, and low molecular weight by-products were removed using a dialysis bag with a cutoff molecular weight of 10 kDa. Subsequently, dextran gel chromatography (Sephadex G-50) was employed to eliminate free Cur and Lf, resulting in the purification of Lf-Cur-LCL.

2.3 High-performance liquid chromatography (HPLC) detection method

In terms of detection of Cur with HPLC, we performed this analysis in house using an LC-20AD system (Shimadzu, Japan) equipped with a Symmetry C18 column (5 μm, 4.6 mm × 250 mm; Merck KGaA, Germany) maintained at 30 °C. The mobile phase comprised acetonitrile and 4% glacial acetic acid solution (48 : 52, v/v) at a flow rate of 1.0 mL minute^{-1}, with detection carried out at 430 nm and an injection volume of 20 μL. Standard Cur solutions (0.01–100 μg mL^{-1}) were prepared in chromatography-grade methanol and injected in triplicate to construct the calibration curve by plotting the peak area (Y) against Cur concentration (X). For plasma sample preparation, blood (0.5 mL) was collected from the rat orbital venous plexus and incubated at 37 °C for 20 minutes, followed by centrifugation at 3700 revolutions minute^{-1} for 10 minutes to obtain plasma, which was stored at −80 °C until use. Aliquots of plasma (200 μL) were transferred into 1.5 mL EP tubes containing anticoagulant and ascorbic acid, followed by the addition of 40 μL demethoxycurcumin (DMC, internal standard) and Cur solutions of different concentrations (0.05–20 μg mL^{-1}). Extraction was carried out twice with aliquot (600 μL) of cold diethyl ether by vortexing for 1 minute and centrifuging at 10 000 revolutions minute^{-1} for 5 minutes at 4 °C. The combined ether layers were evaporated to dryness under a gentle stream of nitrogen at 37 °C, and the residue was reconstituted in aliquot (200 μL) of cold methanol, vortexed, and centrifuged at 10 000 revolutions minute^{-1} for 10 minutes. The resulting supernatant was injected into the HPLC system for analysis. The ratio of Cur to IS peak areas (Y) was plotted against the corresponding Cur concentrations (X) to generate the *in vivo* calibration curve, with the regression equation $Y = 0.0408X - 0.0048$ ($R^2 = 0.9977$) used for quantification.

2.4 Liposomal characterization

2.4.1 PS and zeta potential (ZP). Appropriate amounts of Cur-L, Cur-LCL, and Lf-Cur-LCL solutions were placed in a cuvette. The PS distribution and ZP of these solutions were

Open Access Article. Published on 07 November 2025. Downloaded on 1/9/2026 2:42:34 PM. This article is licensed under a Creative Commons Attribution-NonCommercial 3.0 Unported Licence.

measured at room temperature using a Brookhaven 90 Plus Particle Size Analyzer and PALS instrument as described in previous work.[44]

2.4.2 Morphology observation. Cur-L, Cur-LCL, and Lf-Cur-LCL were diluted to approximately 100 μg mL^{-1} using double-distilled water. A drop of each diluted solution was placed on a copper grid and stained with 2% phosphotungstic acid. The morphology of the samples was then examined using TEM.

2.4.3 Encapsulation efficiency (EE) and drug loading (DL). The EE of the liposomes was determined using dextran gel chromatography.[45] A chromatography column was packed with 50 g of Sephadex G-50 and equilibrated with water. Then, 1 mL of the prepared micelles (1 mg mL^{-1}) was carefully added to the top of the column and eluted with purified water. The eluate was collected in fractions of 10 mL each and analyzed with HPLC to determine the Cur content that was encapsulated in the nanoliposomes. Once Cur was no longer detectable in the purified water eluate, the elution was switched to 0.2% sodium chloride solution to detect the unencapsulated Cur.

The DL was determined by taking the 1 mg mL^{-1} formulation, filtering it through a 0.22 μm organic membrane before analysis *via* the HPLC method.

$$\mathrm{EE}(\%) = \frac{W_{\text{encapsulated}}}{W_{\text{encapsulated}} + W_{\text{unencapsulated}}} \times 100\% \quad (1)$$

$$\mathrm{DL}(\%) = \frac{W_{\text{encapsulated}}}{M} \times 100\% \quad (2)$$

The amount of Cur encapsulated into liposomes and unencapsulated Cur was respectively denoted as $W_{\text{encapsulated}}$ and $W_{\text{unencapsulated}}$, whilst the total amount of liposomes was denoted as M.

2.4.4 Storage stability. The prepared Cur-L, Cur-LCL, and Lf-Cur-LCL were stored in sealed containers at room temperature (25 °C) and 4 °C for one week. Samples were taken on days 0, 3, and 7 to observe the appearance and measure the PS distribution, PDI and ZP.

2.4.5 *In vitro* release study. The *in vitro* release behavior of Cur, Cur-L, Cur-LCL, and Lf-Cur-LCL was investigated using the dialysis method in in three different buffer solutions of pH 1.2, pH 6.8, and pH 7.4. Raw drug (1 mg, dissolved in a small amount of methanol) and formulations (1 mg, dissolved in 1 mL of purified water) were placed in dialysis bags (MW = 3500 Da). After we have securely tied both ends of the dialysis bags, they were placed in 100 mL of release medium in an Erlenmeyer flask and shaken in an incubator shaker (37 °C, 100 revolutions minute^{-1}). Samples of 1 mL were taken out at 5, 15, 30, 45, 60, 90, 120, 180, 240, 360, 480, 600, 720, 1440, 2160, and 2880 minutes using a pipette. Each time the sample was taken, 1 mL of fresh release medium was added back. The collected samples were diluted with methanol and analyzed using the previously described HPLC method.

2.5 Cellular uptake study

PC12 neural cells were selected for the liposomal cellular uptake experiment *in vitro* as stated in previous work.[46] The cells were seeded at a density of 1×10^5 cells mL^{-1}, and cultured at 0.1 mL per well for 24 hours. The cells were then incubated with complete medium containing 10 μg mL^{-1} of Cur-L, Cur-LCL, Lf-Cur-LCL and Lf-Cur-LCL + Lf treatment. The blank control group was incubated with complete medium. For the Lf-Cur-LCL + Lf treatment group, the cells were first treated with Lf for a certain period to allow the Lf to interact with the cells. After that, the cells were treated with the Lf-Cur-LCL formulation.

After incubation, the cells were treated at 37 °C for 4, 12, and 24 hours, and then washed three times with cold PBS, 5 minutes each time. To allow the dosage forms to permeabilize and access the interior of the cells, we treated the cells with 1% Triton X-100 for 45 min. The cells were then stained with Hoechst 33342 for 10 minutes at room temperature to visualize the nuclei. Afterward, the cells were washed again with PBS. The cellular uptake of the liposomes was observed using a fluorescence microscope. Hoechst-stained nuclei were visible under blue fluorescence (excitation at 350 nm and emission at 461 nm), and the fluorescence of the drug was detected through the appropriate channels. Images were captured at 4, 12, and 24 hours.

2.6 Quantitative analysis by flow cytometry

The uptake of various curcumin formulations by PC12 cells was quantitatively analyzed using flow cytometry. Cells were treated with the different formulations for 4, 12, and 24 hours. After incubation, they were washed thoroughly with PBS, detached, and resuspended as a single-cell suspension. The intrinsic fluorescence of intracellular curcumin was measured directly using a BD FACSCalibur flow cytometer (BD Biosciences, USA) with a 488 nm laser for excitation and a 530/30 nm filter for emission detection. The median fluorescence intensity (MFI) of the gated single-cell population was recorded for each sample and time point, with the MFI from untreated cells used to establish the autofluorescence baseline. The resulting MFI values served as a direct metric for the quantitative comparison of cellular uptake over time.

2.7 *In vivo* pharmacokinetics

Twenty SD rats were acclimatized in the laboratory environment for three days before the experiment. The rats were randomly divided into four groups ($n = 5$). We withheld food from the rats for 12 hours before the experiment, while access to water was maintained. Each group was administered 10 mg kg^{-1} of Cur, Cur-L, Cur-LCL and Lf-Cur-LCL *via* tail vein injection.[47] Blood samples were collected from the retro-orbital plexus of the rats' eyes at various time points. After processing the blood samples, we analyzed them with HPLC to determine plasma drug concentration and calculate the pharmacokinetic parameters.

2.8 Tissue distribution

Based on existing literature, sixty-four mice were randomly divided into four groups ($n = 16$), namely Cur, Cur-L, Cur-LCL and Lf-Cur-LCL groups.[48] After administering 10 mg kg^{-1} of the dosage forms *via* tail vein injection to the mice, four mice from each group were euthanized by decapitation at 0.5, 4, 8,

 © 2026 The Author(s). Published by the Royal Society of Chemistry

Open Access Article. Published on 07 November 2025. Downloaded on 1/9/2026 2:42:34 PM. This article is licensed under a Creative Commons Attribution-NonCommercial 3.0 Unported Licence.

and 12 h post-injection.[47] The heart, liver, spleen, lungs, kidneys, and brain of the mice were immediately harvested. The tissues were blotted dry with filter paper to remove moisture, weighed, and recorded. Different amounts of 0.9% NaCl solution (0.2 g mL^{-1}) were added to the EP tubes containing the tissues, such that for 0.2 g of tissue, while 1 mL of 0.9% NaCl was added. The tissues were homogenized using a high-speed homogenizer to produce tissue homogenates. In a 1.5 mL EP tube, an aliquot (100 μL) of tissue homogenate was mixed with 900 μL of diethyl ether to ensure extraction of the drug. The mixture was vortexed for 2 min and then centrifuged at 10 000 revolutions $minute^{-1}$ and 4 °C for 10 minutes. The ether phase was transferred to a new EP tube and evaporated to dryness under nitrogen at 25 °C. The residue was reconstituted in an aliquot (100 μL) of HPLC-grade methanol, vortexed, and centrifuged at 12 000 revolutions $minute^{-1}$ and 4 °C for 10 minutes. Finally, the supernatant was collected and analyzed *via* HPLC detection.

2.9 Therapeutic effects on CIH mice

2.9.1 Groupings. Six-week-old specific pathogen free-grade C57BL/6 male mice were acclimatized for one week before they were randomly divided into the following groups ($n = 6$):

(a) Normal control group (NC): the mice in this group received no treatment.

(b) Model group (M): the model was constructed in the hypoxia chamber for 4 weeks without medical intervention as stated in existing literature.[49]

(c) Low-dose Cur group (Cur-5): starting from day 1 (synchronous with the modeling mice), the mice received tail vein injections of Cur at 5 mg kg^{-1} every other day for four weeks.

(d) High-dose Cur group (Cur-10): starting from day 1 (synchronous with the modeling mice), the mice received tail vein injections of Cur at 10 mg kg^{-1} every other day for four weeks.

(e) Low-dose Cur-L group (Cur-L-5): starting from day 1 (synchronous with the modeling mice), the mice received tail vein injections of Cur-L at 5 mg kg^{-1} every other day for four weeks.

(f) High-dose Cur-L group (Cur-L-10): starting from day 1 (synchronous with the modeling mice), the mice received tail vein injections of Cur-L at 10 mg kg^{-1} every other day for four weeks.

(g) Low-dose Cur-LCL group (Cur-LCL-5): starting from day 1 (synchronous with the modeling mice), the mice received tail vein injections of Cur-LCL at 5 mg kg^{-1} every other day for four weeks.

(h) High-dose Cur-LCL group (Cur-LCL-10): starting from day 1 (synchronous with the modeling mice), the mice received tail vein injections of Cur-LCL at 10 mg kg^{-1} every other day for four weeks.

(i) Low-dose Lf-Cur-LCL group (Lf-Cur-LCL-5): starting from day 1 (synchronous with the modeling mice), the mice received tail vein injections of Lf-Cur-LCL at 5 mg kg^{-1} every other day for four weeks.

(j) High-dose Lf-Cur-LCL group (Lf-Cur-LCL-10): starting from day 1 (synchronous with the modeling mice), the mice received tail vein injections of Lf-Cur-LCL at 10 mg kg^{-1} every other day for four weeks.

2.9.2 Establishment of the CIH animal model. During the experiment, the mice in the experimental chamber experienced hypoxia due to the limited oxygen when the chamber was sealed. When the chamber was opened, air rapidly entered, causing reoxygenation. Each cycle lasted 150 seconds (120 seconds sealed and 30 seconds open), for 8 hours daily (10:00 AM to 6:00 PM). The control group mice were placed in a control chamber under identical conditions except for the lack of hypoxia exposure. This process continued for four weeks. The oxygen concentration inside and outside the experimental chamber was monitored using a CYS digital oxygen meter (Shanghai Yuyan Instruments Co., Ltd). During the experimental period, the mice were deprived of food and water, and their respiratory rate, sleep conditions, and tail arterial blood oxygen saturation were monitored. Normal diet was resumed during non-experimental periods.

2.9.3 Detection

2.9.3.1 Blood gas analysis. On the last day of hypoxia, ten groups of mice designated for subsequent experiments were anesthetized with an intraperitoneal injection of 10% urethane. Immediately after anesthesia, the chest cavity was opened to expose the heart, and 0.2 mL of arterial blood was drawn from the abdominal aorta using a 1 mL heparinized syringe. The blood gas values were measured, which included oxygen partial pressure (PO_2) and carbon dioxide partial pressure (PCO_2).

2.9.3.2 Physicochemical indicators. An appropriate amount of mouse brain tissue was homogenized with physiological saline to create a tissue homogenate. The homogenate was centrifuged, while the supernatant was collected. The levels of MDA and SOD in the mouse brain tissue were measured according to the instructions provided with the ELISA kits from Shanghai Yubo Biotechnology Co., Ltd.

2.9.3.3 HE staining. Immediately after blood collection, the mice were euthanized, and their brain, liver, spleen, and lung tissues were dissected. A portion of these tissues was stored in 4% paraformaldehyde solution for preservation. The fixed brain, liver, spleen, and lung tissues were then removed and washed with PBS at pH 7.4. After dehydration, the tissues were embedded in paraffin, sectioned, and stained using an HE staining kit. The stained sections were then photographed under a microscope.

2.9.3.4 Immunohistochemical (IHC) staining. To further evaluate the therapeutic effects on brain tissue, immunohistochemical (IHC) staining was performed to detect the expression of relevant biomarkers, including caspase 3, Bcl-2, and Bax, which are associated with apoptosis. After fixation in 4% paraformaldehyde and embedding in paraffin, tissue sections were incubated overnight at 4 °C with primary antibodies specific to caspase 3, Bcl-2, and Bax. The sections were then treated with secondary antibodies and visualized using a DAB detection system.

Open Access Article. Published on 07 November 2025. Downloaded on 1/9/2026 2:42:34 PM.
This article is licensed under a Creative Commons Attribution-NonCommercial 3.0 Unported Licence.

2.10 Statistical analysis

Data were analyzed using SPSS 21.0 statistical software. The measurement data that conformed to a normal distribution were expressed as mean ± standard deviation ($x \pm s$), whereas measurement data that did not conform to a normal distribution were presented as the median and interquartile range. Comparisons of measurement data between two groups were performed using an independent sample *t*-test. Categorical data are presented as [*n* (%)], while comparisons between groups for categorical data were performed using the χ^2 test. Spearman correlation analysis was used to perform the correlation. A $P < 0.05$ was considered statistically significant.

3 Results and discussion

3.1 Establishment of *in vitro* and *in vivo* analysis methods for Cur

The validated HPLC methods for both *in vitro* and *in vivo* analyses were applied to various experimental setups, including EE, DL, and pharmacokinetic studies. The high specificity and sensitivity of the method allowed for precise quantification of Cur in different formulations and biological matrices. The ability to measure Cur at low concentrations in plasma is particularly significant for pharmacokinetic studies, which require tracking the drug's concentration over time to understand its absorption, distribution, metabolism, and excretion (ADME) profile. As shown in Fig. 1A, the retention time for Cur was approximately 6.2 min. This retention time was appropriate, with no interference from solvent peaks, and exhibited good peak shape and separation, indicating high specificity of this analytical method for determining Cur content. The linear regression equation for Cur was $Y = 147114X - 125177$, with an R^2 value of 0.9991. This demonstrates good linearity in the concentration range of 0.01 to 100 μg mL^{-1}, thus making it suitable for *in vitro* quantitative detection of Cur.

As illustrated in the chromatograms of Fig. 1B and C, the internal standard and Cur peaked at approximately 4.4 min and 6.2 min, respectively. The solvent, internal standard, and drug peaks were well separated from each other, with no interference from endogenous substances. The *in vivo* standard curve equation for Cur was $Y = 0.0408X - 0.0048$ with $R^2 = 0.9977$, which indicates a good linear relationship ($R^2 > 0.99$) in the concentration range of 0.05 to 20 μg mL^{-1}, and can be used for determining Cur content *in vivo*. It is a known fact that Cur is poorly soluble in water and is rapidly degraded at physiological pH.[50] Although these and other factors obviously affect determination of Cur concentration in samples, existing literature suggests that HPLC can determine Cur in several samples at varied concentration ranges with some reported HPLC methods having limits of detection and quantification within nanogram per liter (ng L^{-1}).[51] These studies used similar chromatographic conditions like ours and hence we are certain that our established analytical method is reliable and feasible to determine lower concentrations of Cur in our samples. To ensure the accuracy of our pharmacokinetic data, we put in place some standard operating procedures during the analysis to ensure that we limit the effects of these factors on the *in vivo* analyses.

3.2 Characterization of Cur liposomes

The PS and PDI are pivotal parameters in evaluating the quality and stability of liposomal formulations.[52] The ZP, which is indicative of the surface charge of liposomes, provides valuable insight into their stability in suspension. Furthermore, EE and DL are critical metrics that determine the efficacy of the liposomal drug delivery system.[53] The PS, PDI, ZP, EE and DL of Cur-L, Cur-LCL and Lf-Cur-LCL are presented in Table 1. In this study, the PS for Cur-L, Cur-LCL, and Lf-Cur-LCL was found to be 168.26 ± 2.75 nm, 181.71 ± 3.59 nm, and 205.64 ± 3.83 nm, respectively. The increase in the liposomal PS from Cur-L to Lf-Cur-LCL may be attributed to the addition of polyethylene glycol (PEG) and Lf modifications, which added to the surface complexity and overall size of the liposomes. Despite the increase, the particle sizes remained within an acceptable range for systemic circulation and effective delivery to the target tissues. In support of this result, Teixeira and colleagues developed brain-targeted Riluzole-loaded nanoparticles with the mean PS ranging from 147.2 nm to 203.1 nm.[54]

The PDI values for all formulations were below 0.25, indicating a narrow size distribution and homogeneity. Specifically, the PDI values were 0.211 ± 0.005 for Cur-L, 0.226 ± 0.011 for Cur-LCL, and 0.244 ± 0.010 for Lf-Cur-LCL. Low PDI values are indicative of a uniform liposomal size, which is essential for the predictability of pharmacokinetics and biodistribution. Additionally, the respective mean ZP values for Cur-L, Cur-LCL and Lf-Cur-LCL were −27.65 ± 1.06, −26.16 ± 0.52 and −24.59 ± 0.75. In particular, characteristics of pharmacokinetics are directly affected by the PS and PDI, which impact the amount of Cur that was loaded into liposomes and can be released and absorbed after the nanoparticles have reached their target site.[55] As an indicator that reflects particle surface charge, ZP can serve

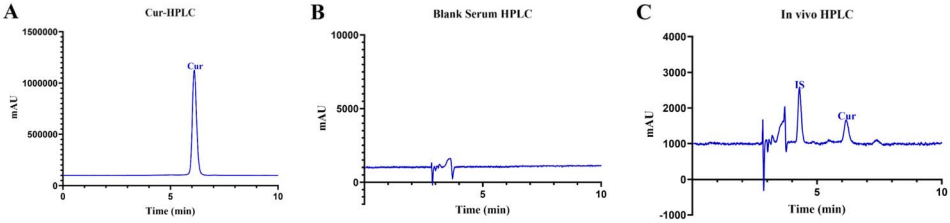

Fig. 1 High-performance liquid chromatographic (HPLC) assay of curcumin (Cur) *in vitro* (A), HPLC assay of blank serum (B), and HPLC assay of the *in vivo* sample (C).

© 2026 The Author(s). Published by the Royal Society of Chemistry

Open Access Article. Published on 07 November 2025. Downloaded on 1/9/2026 2:42:34 PM.
This article is licensed under a Creative Commons Attribution-NonCommercial 3.0 Unported Licence.

Table 1 Characterization results of different liposomes

Liposomes	PS (nm)	PDI	ZP (mV)	EE (%)	DL (%)
Cur-L	168.26 ± 2.75	0.211 ± 0.005	−27.65 ± 1.06	92.38 ± 1.26%	7.32 ± 0.27%
Cur-LCL	181.71 ± 3.59	0.226 ± 0.011	−26.16 ± 0.52	91.55 ± 1.15%	7.65 ± 0.31%
Lf-Cur-LCL	205.64 ± 3.83	0.244 ± 0.010	−24.59 ± 0.75	95.67 ± 1.01%	4.17 ± 0.25%

as a vital index of stability of dispersed colloidal systems like liposomes.[56] When the absolute value of ZP is larger, it suggests higher repulsion within particles that are adjacent to each other, which further indicates that the particles do not aggregate easily and settle as well as implying the increased stability of the liposomal systems.[57,58] Our developed liposomes seem to resemble an ideal liposomal system, which scientists predict that it should display high a ZP value, narrow and low PDI and smaller-sized particles.[59]

The EE% and DL% are critical parameters that determine the effectiveness of the liposomal drug delivery system. The EE% values for Cur-L, Cur-LCL, and Lf-Cur-LCL were 92.38 ± 1.26%, 91.55 ± 1.15%, and 95.67 ± 1.01%, respectively, demonstrating high encapsulation rates. The slightly higher EE in Lf-Cur-LCL could be due to the additional binding affinity provided by the Lf modification, which may enhance Cur encapsulation.[60] The DL% values for Cur-L, Cur-LCL, and Lf-Cur-LCL were 7.32 ± 0.27%, 7.65 ± 0.31%, and 4.17 ± 0.25%, respectively. While the DL% of Lf-Cur-LCL was lower than that of the other formulations, the high EE% compensates for this, thus ensuring a sufficient amount of Cur was delivered to the target site.

As shown in Fig. 2, Cur-L, Cur-LCL and Lf-Cur-LCL exhibited a near-spherical shape with a PS around 200 nm. This spherical morphology is advantageous for systemic circulation and cellular uptake, as it can enhance the stability and reduce the clearance by the RES.[61] The results of PS measurement are basically consistent with the data that were measured with TEM.

The characterization of the liposomal formulations (Cur-L, Cur-LCL, and Lf-Cur-LCL) demonstrated excellent properties in terms of PS, PDI, ZP, EE%, DL%, morphology, and stability. Importantly, the EE, lamellarity, surface charges, and PS have been discovered to highly influence the properties of liposomes, and hence these factors should be considered when designing liposomes for targeted delivery. The slight variations in these parameters suggest that PEGylation and Lf modification did not adversely affect the overall quality and stability of the formulations. These findings confirm that the liposomal formulations are well-suited for delivering Cur effectively, particularly Lf-Cur-LCL, which showed enhanced brain-targeting capabilities. The comprehensive characterization lays a solid foundation for their potential clinical application in treating hypoxic brain injury and other related conditions. Importantly, we understand that molecular-level analysis is essential for understanding the structural and functional characteristics of curcumin-loaded liposomes, which directly impact their stability, bioavailability, and therapeutic efficacy. Techniques such as Fourier-transform infrared spectroscopy (FTIR), differential scanning calorimetry (DSC), and nuclear magnetic resonance (NMR) spectroscopy help elucidate the interactions between Cur and liposomal lipids, confirming encapsulation

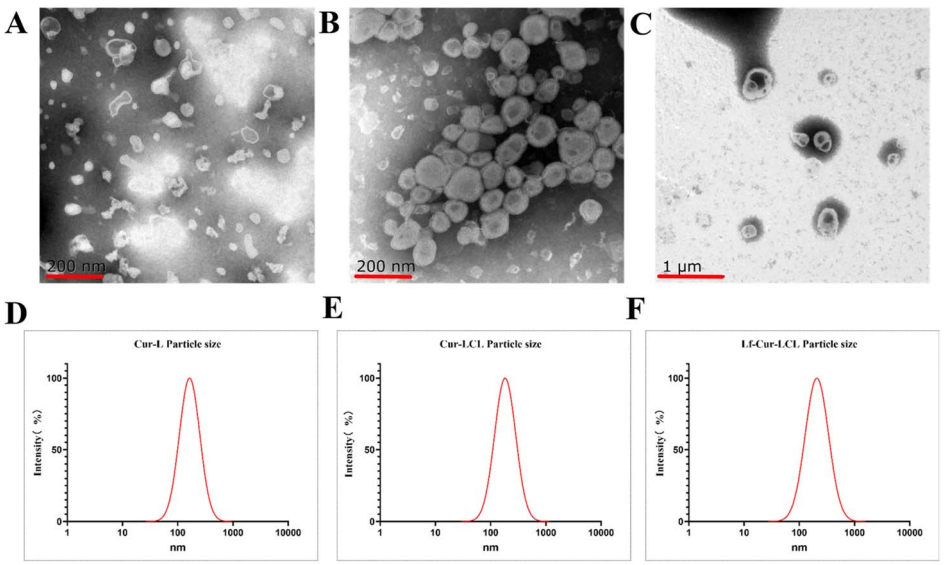

Fig. 2 Transmission electron microscopy (TEM) image of curcumin liposomes (Cur-L), scale bar = 200 nm (A); TEM image of curcumin long-circulating liposomes (Cur-LCL), scale bar = 200 nm (B); TEM image of lactoferrin modified long-circulating liposomes (Lf-Cur-LCL), scale bar = 1 μm (C); PS test results of Cur-L (D); PS test results of Cur-LCL (E); PS test results of Lf-Cur-LCL (F).

Open Access Article. Published on 07 November 2025. Downloaded on 1/9/2026 2:42:34 PM.
This article is licensed under a Creative Commons Attribution-NonCommercial 3.0 Unported Licence.

and structural integrity. These analyses also provide insights into the release kinetics, crystallinity, and physicochemical stability, enabling researchers to optimize liposomal formulations for improved drug delivery and biological performance. Besides, existing literature has attempted to explain the structure, interactions, and conformational changes of Cur and the liposome's lipid bilayer.[62,63] Notwithstanding, we will perform a comprehensive molecular-level analysis of the physicochemical properties of Cur liposomes in our not-too-distant investigations to completely understand their structure, interactions, and conformational changes.

3.3 *In vitro* cumulative release

To predict the efficacy of drugs *in vivo* and provide a reference for the dosage regimen, it is important that we evaluate the quality of formulations by examining the profile of drug release. As shown in Fig. 3, the cumulative release rate of Cur was significantly lower than that of Cur-L, Cur-LCL and Lf-Cur-LCL. Among the three-release media, Cur reached its highest release point after 4 hours, with a release rate not exceeding 35% within 12 hours. In contrast, Cur-L, Cur-LCL and Lf-Cur-LCL reached their peak cumulative release at 10 (8 in pH 7.4), 24, and 36 hours, respectively, demonstrating excellent sustained-release properties, particularly for the Lf-Cur-LCL formulation. The cumulative release of Cur in pH 1.2 medium was about 18.24%, while in pH 7.4 medium it was approximately 24.92%. Statistical results showed that the cumulative release of Cur in pH 7.4 medium was significantly higher than that in pH 1.2 medium, ($p < 0.01$). Overall, the release rate of Cur and its formulations was rapid in pH 7.4 PBS medium, with the highest cumulative release rate being observed at this pH. With regard to Cur liposomes, all the formulations exhibited sustained release with a higher release rate being discovered in pH 7.4 PBS medium, which aligned with existing literature.[64] This observation may be attributed to the pH-dependent solubility and stability of Cur and structural integrity of the liposomal carrier. The deprotonation of the phenolic moiety of Cur facilitates its partitioning into aqueous environments, resulting in increased solubility under neutral to alkaline conditions. Conversely, the protonation of these groups under acidic conditions (pH 1.2) reduces solubility due to enhanced intermolecular hydrogen bonding.[65] Although the chemical instability of Cur in neutral to alkaline media may lead to partial degradation following release, which could compromise the cumulative release measurement, it still retains a relatively high apparent cumulative release rate. The structural integrity of liposomes is influenced by pH levels; at pH 7.4, this increased membrane fluidity and permeability further facilitates the release of Cur.[66] Consequently, the highest cumulative release of Cur was observed in PBS at pH 7.4. Furthermore, in all pH media, the drug showed a certain downward trend in cumulative release after reaching the maximum cumulative release amount. This phenomenon was presumably due to the growth or transformation of the drug's crystal form during the *in vitro* release process, which may have led to a decrease in solubility. The time points of decline in the cumulative release rate were extended in sequence in the order of Cur, Cur-L, Cur-LCL and Lf-Cur-LCL, which reflected the good encapsulation of the drug by the liposomes and the crystal inhibition effect of the formulation carriers on the drug.[67] The sustained release profiles observed in this study have significant implications for the therapeutic efficacy of Cur formulations. Sustained release helps maintain consistent drug levels in the bloodstream, which is crucial for chronic conditions like hypoxic brain injury. The ability of Lf-Cur-LCL to release Cur over an extended period enhances its potential as a therapeutic agent, thereby providing prolonged neuroprotection and mitigating oxidative stress associated with hypoxia.

3.4 Stability assessment results

Stability assessment is crucial for ensuring that formulations remain effective during storage and transportation. The stability of liposomes is influenced by several factors, which include but are not limited to their surface features, shape, size, and type of materials that were employed for the preparation of the delivery system.[68] As shown in Table 2, Cur-L stored at 4 °C for 7 days exhibited no significant changes in PDI, ZP and PS ($P > 0.05$). When stored at 25 °C for 7 days, Cur-L also showed no significant changes in PDI and ZP ($P > 0.05$), although the PS increased from 167.51 nm to 171.43 nm ($P < 0.05$), a change rate of approximately 2.34%, which is still within an acceptable range. As indicated in Table 3, Cur-LCL stored at both 4 °C and 25 °C for 7 days showed no significant changes in PDI, ZP, and PS ($P > 0.05$), with a slight increase in the PS of about 1.63% at the temperature of 25 °C on the 7th day. As presented in Table 4,

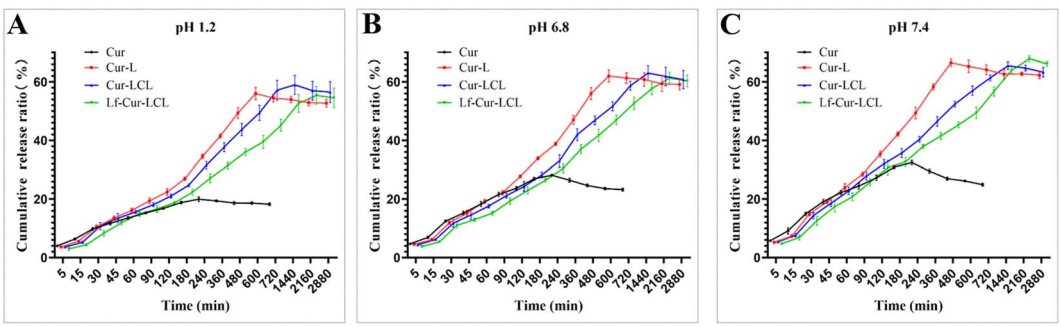

Fig. 3 *In vitro* cumulative release curves of curcumin liposomes (Cur-L), Cur-LCL and lactoferrin (Lf)-Cur-LCL in various media ((A) pH 1.2, (B) pH 6.8, and (C) pH 7.4; $n = 3$).

© 2026 The Author(s). Published by the Royal Society of Chemistry

Open Access Article. Published on 07 November 2025. Downloaded on 1/9/2026 2:42:34 PM.
This article is licensed under a Creative Commons Attribution-NonCommercial 3.0 Unported Licence.

Table 2 Stability assessment results of curcumin liposomes (Cur-L)[a]

	Cur-L					
	PDI		ZP (mV)		PS (nm)	
Day	4 °C	25 °C	4 °C	25 °C	4 °C	25 °C
0	0.212 ± 0.005	0.213 ± 0.006	−27.37 ± 0.87	−27.11 ± 0.55	168.83 ± 3.38	167.51 ± 3.87
3	0.218 ± 0.006	0.218 ± 0.009	−27.78 ± 0.76	−28.12 ± 0.67	166.31 ± 3.61	169.57 ± 2.12
7	0.209 ± 0.004	0.221 ± 0.008	−27.89 ± 0.98	−27.87 ± 0.12	169.61 ± 3.14	171.43 ± 3.29*

[a] PDI: polymer dispersity index, ZP: zeta potential, and PS: particle size.

Lf-Cur-LCL stored at 4 °C for 7 days showed no significant changes in PDI, ZP and PS ($P > 0.05$). When it was stored at 25 °C for 7 days, Lf-Cur-LCL exhibited no significant changes in PDI and ZP ($P > 0.05$), while the PS increased from 205.29 nm to 209.87 nm ($P < 0.05$), a change rate of approximately 2.23%, which was still within an acceptable range. These results indicate that all three formulations exhibited good stability when stored at 4 °C and 25 °C for 7 days. Notwithstanding, future studies will assess the long-term storage stability of these formulations at higher temperatures and relative humidities.

3.5 Cellular uptake results

Cellular uptake studies are crucial for understanding how effectively drug delivery systems can transport therapeutic agents into target cells. The results of the *in vitro* cellular uptake experiments are shown in Fig. 4A–D. It can be observed that the fluorescence intensity of Cur-L, Cur-LCL and Lf-Cur-LCL in P12 cells increased gradually over time, thus indicating increased cellular uptake. This finding demonstrates that P12 cells took up more of the three drug delivery systems as time progressed.

At the same time points, the fluorescence intensities of Cur-LCL and Lf-Cur-LCL were significantly higher than that of Cur-L, which suggests that long-circulating liposomes and Lf-modified long-circulating liposomes were more conducive to phagocytosis by P12 cells. This observation indicates that Cur could be delivered effectively to PC12 cells, thus potentially enhancing its activity. However, this study did not investigate the effects of liposomal size and PS changes on cellular uptake.

The cellular uptake study highlights the superior performance of Cur-LCL and Lf-Cur-LCL in delivering Cur to PC12 neural cells. PEGylation and Lf modification could significantly enhance the uptake efficiency compared to that of conventional Cur liposomes.[69,70] The addition of PEG to the liposomes creates a "stealth" effect, thus reducing opsonization and recognition by the RES.[71] This prolongs the circulation time of the liposomes, thereby increasing the probability of cellular uptake. Lf is a glycoprotein that can bind to Lf receptors expressed on the surface of many cell types, including neurons. The modification of Cur-LCL with Lf facilitates receptor-mediated endocytosis, a process by which the liposomes are actively transported into the cells. These findings underscore the potential of Lf-Cur-LCL as an effective brain-targeting drug delivery system for treating hypoxic brain injury and other neurological disorders. The enhanced uptake ensures higher intracellular concentrations of Cur, which is critical for achieving therapeutic efficacy.

To complement the qualitative fluorescence imaging, the cellular uptake was quantitatively analyzed using flow cytometry. As quantitatively detailed in Fig. 4E, the percentage of curcumin-positive PC12 cells demonstrated a clear time- and formulation-dependent increase. Consistent with the microscopic observations, the uptake efficiency followed the following order: Lf-Cur-LCL > Cur-LCL > Cur-L. At the 24 hour time point, the cellular uptake of Lf-Cur-LCL was significantly higher than that of all other formulations. Crucially, the enhanced uptake of Lf-Cur-LCL was effectively inhibited by pre-incubation with an excess of free lactoferrin (Lf-Cur-LCL + Lf group), as the free Lf competitively bound to the Lf receptors on the cell surface. This result provides strong quantitative evidence that the superior cellular internalization of Lf-Cur-LCL is primarily mediated by Lf receptor-specific endocytosis.

In summary, our cellular uptake results show that modifying the liposomes with lactoferrin markedly improved their uptake into PC12 neural cells. The competitive inhibition experiment

Table 3 Stability assessment results of curcumin long-circulating liposomes (Cur-LCL)[a]

	Cur-LCL					
	PDI		ZP (mV)		PS (nm)	
Day	4 °C	25 °C	4 °C	25 °C	4 °C	25 °C
0	0.225 ± 0.007	0.223 ± 0.004	−26.26 ± 0.57	−26.19 ± 0.83	181.83 ± 2.15	181.72 ± 3.51
3	0.228 ± 0.009	0.238 ± 0.009	−26.41 ± 0.75	−26.85 ± 0.89	182.28 ± 2.34	182.47 ± 2.68
7	0.231 ± 0.007	0.238 ± 0.011	−26.17 ± 0.81	−27.35 ± 0.41	182.64 ± 3.61	184.69 ± 3.71

[a] PDI: polymer dispersity index, ZP: zeta potential, and PS: particle size.

Open Access Article. Published on 07 November 2025. Downloaded on 1/9/2026 2:42:34 PM. This article is licensed under a Creative Commons Attribution-NonCommercial 3.0 Unported Licence.

Table 4 Stability assessment results of lactoferrin-modified long-circulating liposomes (Lf-Cur-LCL)[a]

	Lf-cur-LCL					
	PDI		ZP (mV)		PS (nm)	
Day	4 °C	25 °C	4 °C	25 °C	4 °C	25 °C
0	0.243 ± 0.012	0.244 ± 0.011	−24.12 ± 0.45	−24.21 ± 0.24	205.41 ± 3.31	205.29 ± 3.22
3	0.245 ± 0.009	0.251 ± 0.013	−24.35 ± 0.51	−25.17 ± 0.58	205.89 ± 2.93	207.83 ± 4.17
7	0.249 ± 0.009	0.255 ± 0.016	−26.89 ± 0.67	−26.25 ± 0.78	206.18 ± 3.38	209.87 ± 3.55

[a] PDI: polymer dispersity index, ZP: zeta potential, and PS: particle size.

provided clear evidence that this improvement occurs mainly through Lf receptor-mediated endocytosis. Although the PC12 cell model successfully demonstrated the affinity of the formulation for neuronal cells, further studies using more advanced *in vitro* BBB models would help to fully confirm its brain-targeting potential. Together with *in vivo* receptor blocking studies, such approaches could directly measure transcytosis efficiency and offer deeper insight into the active targeting mechanism across the BBB.

3.6 *In vivo* pharmacokinetic results

Pharmacokinetic studies are essential for understanding the ADME of drugs. As shown in Fig. 5, the circulation time of the three formulations *in vivo* is all longer than that of Cur. One hour after tail vein injection, the blood concentrations of the three formulations were higher than that of Cur, with Cur-LCL and Lf-Cur-LCL showing higher blood concentrations than Cur-L. The tail vein injection, which is also known as intravenous injection into the tail vein, is a common route of drug administration that is usually used in animal experiments,[60] particularly in mice and rats. In order for the liposomes to reach target organs such as the brain, heart and lungs *via* liver, scientists usually employ injections *via* the tail vein because it is efficient for large molecules and lipid-based nanoparticles.[72,73] In this work, we chose this method with the aim of getting direct access to systemic circulation, ensuring accurate dosage delivery, minimizing Cur degradation *via* metabolism, preventing potential Lf degradation and causing minimal stress to the animals.[74,75] It is interesting to note that Cur had the shortest circulation time *in vivo*, and thus it became undetectable after 6 hours. In contrast, Cur-L had a circulation time of 12 hours, whilst Cur-LCL and Lf-Cur-LCL had a circulation time of 24 hours. The *in vivo* pharmacokinetic results clearly demonstrated that liposomal formulations, especially Lf-Cur-LCL, significantly prolonged the circulation time of Cur in the bloodstream and exhibited increased blood concentration of Cur, which is expected to further promote the distribution of Cur into the brain. These improvements are critical for achieving sustained therapeutic effects and reducing dosing frequency. The findings underscored the potential of Lf-Cur-LCL as a superior drug delivery system for Cur, particularly for brain-targeted therapies in conditions such as hypoxic brain injury. The enhanced pharmacokinetic profile of Lf-Cur-LCL supports its further development and clinical application.

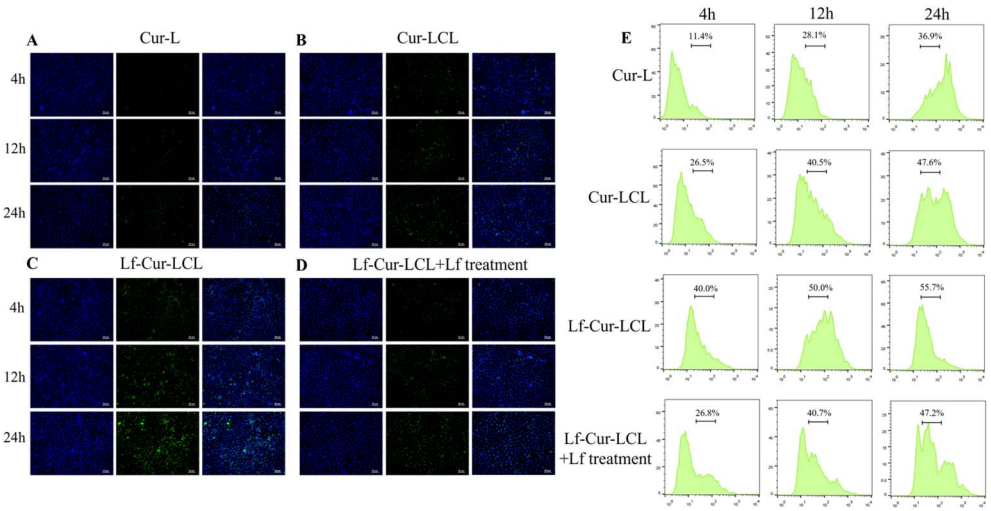

Fig. 4 Phagocytosis results of P12 cells. (A–D) Fluorescence microscopy images of PC12 cells after incubation with (A) Cur-L, (B) Cur-LCL, (C) Lf-Cur-LCL, and (D) Lf-Cur-LCL + Lf for 4, 12, and 24 hours. Scale bar = 50 μm. (E) Quantitative analysis of cellular uptake by flow cytometry. Data are presented as mean ± SD (n = 3).

© 2026 The Author(s). Published by the Royal Society of Chemistry

Open Access Article. Published on 07 November 2025. Downloaded on 1/9/2026 2:42:34 PM.
This article is licensed under a Creative Commons Attribution-NonCommercial 3.0 Unported Licence.

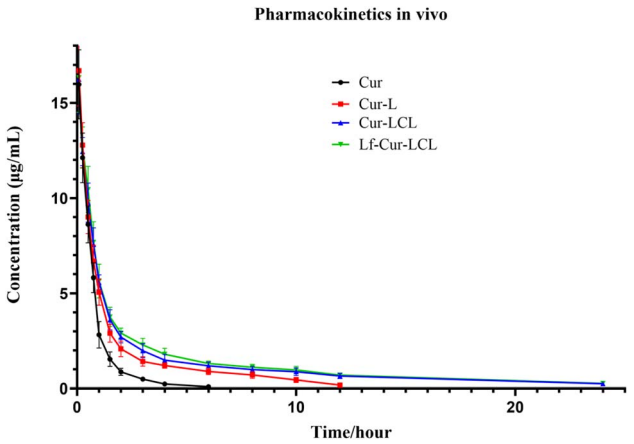

Fig. 5 Concentration–time curve *in vivo*.

3.7 Tissue distribution

Understanding the tissue distribution of a drug is crucial for assessing its therapeutic efficacy and potential toxicity.[76] Although the aim of developing these formulations was to mainly target Cur to the brain, in order to minimize off-target accumulation and avoid potential adverse effects of the liposomes, it is important to understand the biodistribution patterns of Cur-loaded liposomes in other tissues such as the liver, spleen, kidneys, heart, *etc.* As shown in Fig. 6, following tail vein injection of Cur, the highest concentration of Cur was found in the liver and the lowest in the spleen. The concentration of Cur in various organs decreased over time. Notably, Cur remained detectable in the heart, lungs, kidneys, and brain at 8 h, but only for 4 h in the spleen. At 0.5 h, the concentration of Cur in all tissues was higher than that in the Cur-L, Cur-LCL and Lf-Cur-LCL groups. However, starting from the 4th hour, the concentration of Cur was lower than that in the Cur-L, Cur-LCL and Lf-Cur-LCL groups. At the 4th hour, the concentrations of Cur in Cur-LCL and Lf-Cur-LCL groups in the heart, liver, spleen, lungs, and kidneys were still lower than those in the Cur-L group. However, in the 8th and 12th hours, the concentrations of Cur in Cur-LCL and Lf-Cur-LCL groups were higher than those in the Cur-L group. In the 12th hour, the concentration of Cur in the Lf-Cur-LCL group was higher than that in the Cur-LCL group. In brain tissue, starting from 0.5 h, the concentration of Cur in the Lf-Cur-LCL group was consistently higher than in the other groups, thus indicating that Lf-Cur-LCL had superior brain-targeting properties. The superior brain targeting ability of Lf-Cur-LCL was a significant finding. The Lf receptors are abundantly expressed on the BBB, and Lf modification leveraged these receptors to facilitate Cur transport into the brain.[77,78] This targeting capability is crucial for treating neurological disorders, such as hypoxic brain injury, wherein effective drug delivery to the brain is necessary for therapeutic efficacy.

The enhanced and targeted distribution of Lf-Cur-LCL to the brain and other vital organs underscores its therapeutic potential. For neurological conditions, the ability to cross the BBB and achieve higher brain concentrations is crucial.[79] The sustained presence in the liver, spleen, lungs, and kidneys indicates that the formulation could also have applications beyond neurological disorders, thereby potentially addressing systemic conditions requiring extended drug release and targeting. As part of our future work, we intend to corroborate the claim of enhanced brain uptake due to Lf modification by designing experiments using techniques such as *in vivo* imaging, direct brain tissue analysis, and *in vitro* studies of brain endothelial cells to measure uptake and localization Lf-Cur-LCL.[80] We anticipate that these methods can confirm the mechanism of entry and show that Lf-Cur-LCL may be actively transported across the blood–brain barrier (BBB) and accumulate in the brain parenchyma more effectively than unmodified ones like Cur-L and Cur-LCL.[81]

3.8 Therapeutic effect on CIH mice

The CIH is a hallmark of OSA and leads to severe oxidative stress and tissue damage. In the CIH mouse model, PO_2 levels were markedly reduced and PCO_2 levels elevated compared to the blank group ($p < 0.01$), confirming successful model establishment (Fig. 7A and B). Treatment with Cur formulations

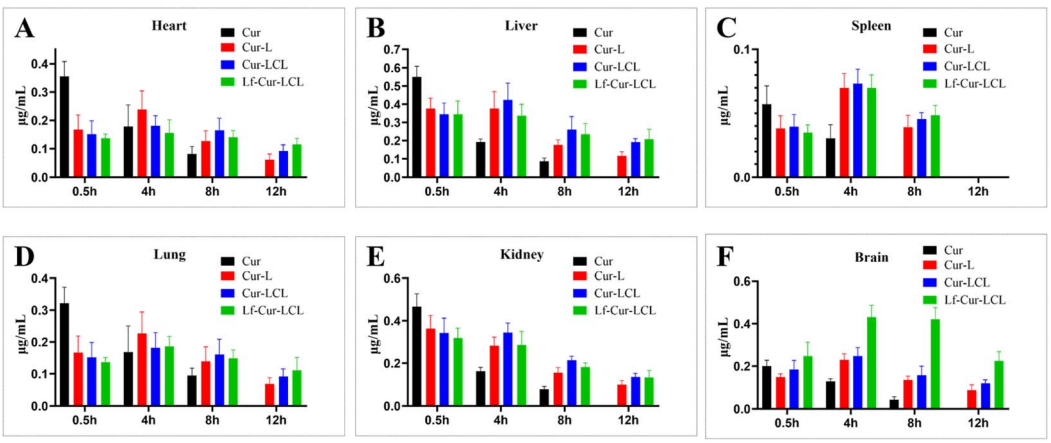

Fig. 6 The distribution of Cur, Cur-L, Cur-LCL and Lf-Cur-LCL in tissues ((A) heart; (B) liver; (C) spleen; (D) lungs; (E) kidney; (F) brain).

Open Access Article. Published on 07 November 2025. Downloaded on 1/9/2026 2:42:34 PM.
This article is licensed under a Creative Commons Attribution-NonCommercial 3.0 Unported Licence.

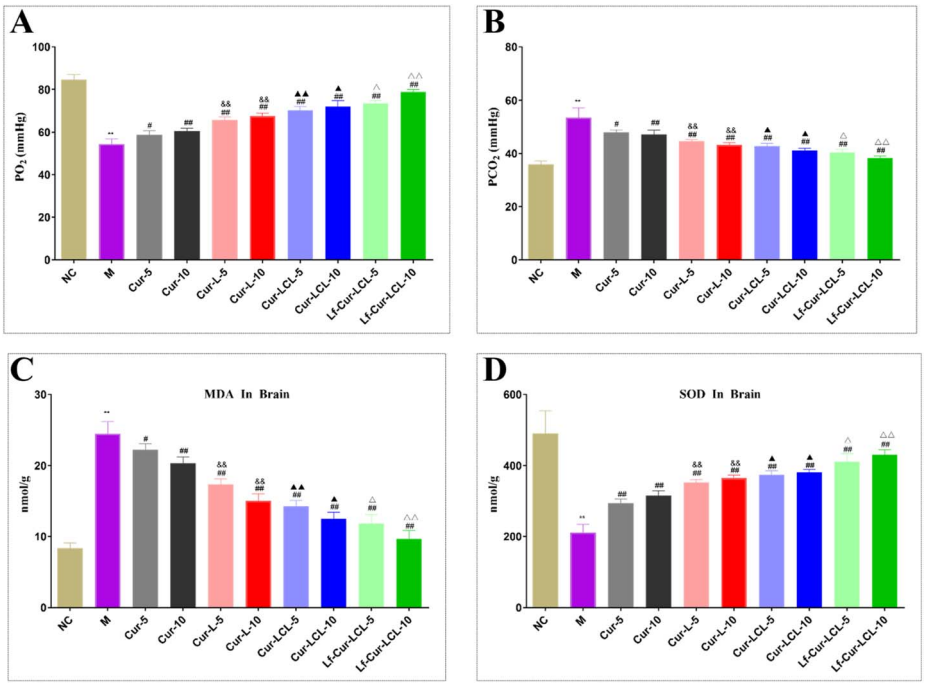

Fig. 7 Detection results of blood gas partial pressure and oxidative markers ((A) Oxygen partial pressure results; (B) carbon dioxide partial pressure results; (C) malondialdehyde (MDA) content results; (D) superoxide dismutase (SOD) content results) (**: compared to the normal control (NC) group, $p < 0.01$; #: compared to the model (M) group, $p < 0.05$; ##: compared to the M group, $p < 0.01$; &&: compared to the same dose of the Cur group, $p < 0.01$; ▲: compared to the same dose of the Cur-L group, $p < 0.05$; ▲▲: compared to the same dose of the Cur-L group, $p < 0.01$; △: compared to the same dose of Cur-LCL, $p < 0.05$; △△: compared to the same dose of Cur-LCL, $p < 0.01$).

significantly improved blood gas parameters, with stepwise enhancement from Cur → Cur-L → Cur-LCL → Lf-Cur-LCL ($p <$ 0.05–0.01). The Lf-Cur-LCL formulation achieved the highest PO_2 increase and greatest PCO_2 reduction, indicating superior efficacy in improving oxygen exchange.

Oxidative stress assessment revealed that MDA, a lipid peroxidation marker, was elevated in CIH mice but significantly reduced by all Cur treatments, with Lf-Cur-LCL showing the strongest decrease ($p < 0.01$) (Fig. 7C). This observation indicates abnormal oxidative stress markers in the CIH mouse model. All Cur treatments significantly reduced MDA levels, with Lf-Cur-LCL showing the most pronounced reduction. This highlights the potent antioxidant properties of the Lf-modified formulation in reducing oxidative stress.

SOD is an important antioxidant enzyme that protects against oxidative damage. SOD activity, which was diminished in the model group, increased markedly after treatment, following the same formulation-dependent trend (Fig. 7D). SOD levels were significantly lower in the model group, which demonstrates impaired antioxidant defense. Treatment with Cur formulations increased SOD levels, with Lf-Cur-LCL achieving the highest increase. This suggests that Lf-Cur-LCL not only reduces oxidative stress but also enhances the antioxidant capacity of the brain tissue.

Overall, Cur-based formulations effectively mitigated CIH-induced oxidative stress and hypoxia, with Lf-Cur-LCL demonstrating the most pronounced therapeutic benefits. The lactoferrin modification enhanced brain targeting and antioxidant capacity, highlighting Lf-Cur-LCL as a promising candidate for treating hypoxic brain injury and related OSA-associated complications.

Currently, weight-loss strategies and airway support (like CPAP) remain the first-line treatment for OSAHS.[82] In the management of residual daytime sleepiness, some pharmacological agents (modafinil/armodafinil and solriamfetol) have primarily been approved,[83] while severity of OSA has been recently reduced *via* weight loss for obese adults using tirzepatide.[84] These treatment options act systemically (weight reduction or wake-promoting) rather than directly increasing drug concentration in the brain. Pharmacological neuroprotectants have preclinically shown promise but their clinical benefit has remained limited and inconsistent.[85] In this context, we aimed to potentially improve brain delivery of the antioxidant/anti-inflammatory agent (Cur) using our developed Lf-Cur-LCL formulation *via* receptor-mediated transcytosis. In comparison with existing clinical options, Lf-Cur-LCL constitutes a mechanistically distinct, targeted approach that could be used to treat CIH-induced OSA. More importantly, while our biodistribution and biomarker data show improved brain exposure and favorable changes in markers of oxidative stress, direct efficacy comparisons of our formulation with approved pharmacological agents require head-to-head functional studies (behavioral/neurological endpoints and safety profiling) and translational toxicology before clinical claims can be made.

As shown in Fig. 8A–D, histopathological examination revealed that CIH induced significant tissue injury across

© 2026 The Author(s). Published by the Royal Society of Chemistry

Open Access Article. Published on 07 November 2025. Downloaded on 1/9/2026 2:42:34 PM.
This article is licensed under a Creative Commons Attribution-NonCommercial 3.0 Unported Licence.

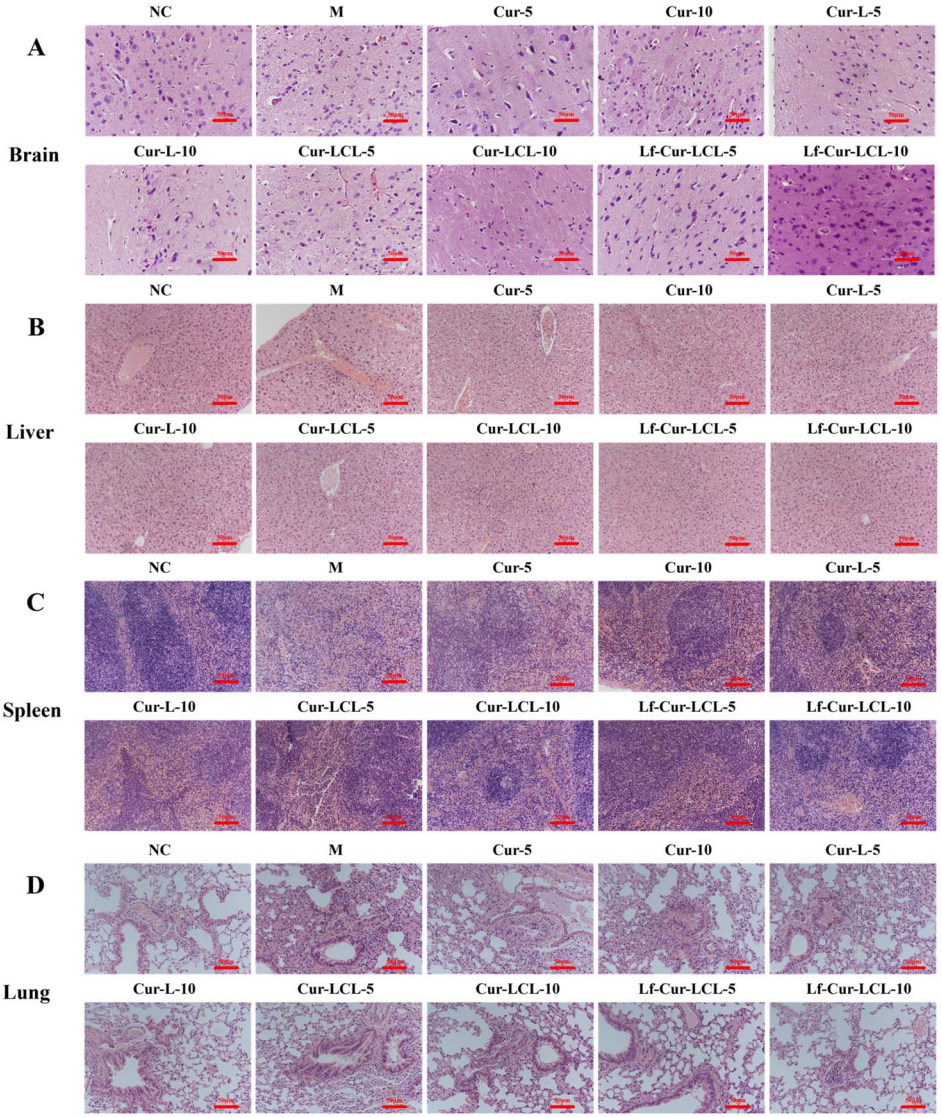

Fig. 8 Histopathological photomicrographs of mouse tissues ((A) brain; (B) liver; (C) spleen; (D) lung) (20×, Scale bar = 50 μm).

multiple organs. In the brain, the model group exhibited pronounced cellular edema, necrosis, and hemorrhage compared to the normal group, which showed intact morphology. Similar pathological alterations, cellular edema, inflammatory infiltration, and nuclear destruction were observed in the liver, spleen, and lungs of CIH mice. Treatment with Cur formulations alleviated these lesions to varying extents, following the trend Cur < Cur-L < Cur-LCL < Lf-Cur-LCL. Notably, Lf-Cur-LCL provided the most significant protection, restoring tissue integrity and reducing inflammation across all examined organs.

The immunohistochemical (IHC) staining results (Fig. 9) of brain tissue revealed significant changes in the expression of apoptotic markers in the treatment groups. Caspase 3, a marker of apoptosis, was significantly reduced in the Lf-Cur-LCL-treated group, indicating decreased apoptosis in brain cells. Bcl-2, an anti-apoptotic protein, showed increased expression in the Lf-Cur-LCL group, suggesting enhanced neuronal survival. Bax, a pro-apoptotic protein, showed reduced expression in the Lf-Cur-LCL group, reflecting a decrease in pro-apoptotic signaling and suggesting improved neuronal protection. These findings support the therapeutic effects of Lf-Cur-LCL, where treatment significantly reduced apoptotic markers and promoted cell survival in brain tissue, leading to enhanced protection against hypoxic brain injury.

The present study demonstrates the therapeutic potential of Lf-Cur-LCL in mitigating brain injury induced by CIH. While these results are promising, our investigation has mainly focused on formulation characterization, pharmacokinetics, and overall therapeutic outcomes. The enhancement in EE observed with the Lf modification, although consistent with other protein-based delivery systems, warrants further mechanistic exploration. Future studies will focus on examining the molecular interactions between Lf and Cur using biophysical techniques such as isothermal titration calorimetry and fluorescence spectroscopy. These approaches will enable detailed

Open Access Article. Published on 07 November 2025. Downloaded on 1/9/2026 2:42:34 PM.
This article is licensed under a Creative Commons Attribution-NonCommercial 3.0 Unported Licence.

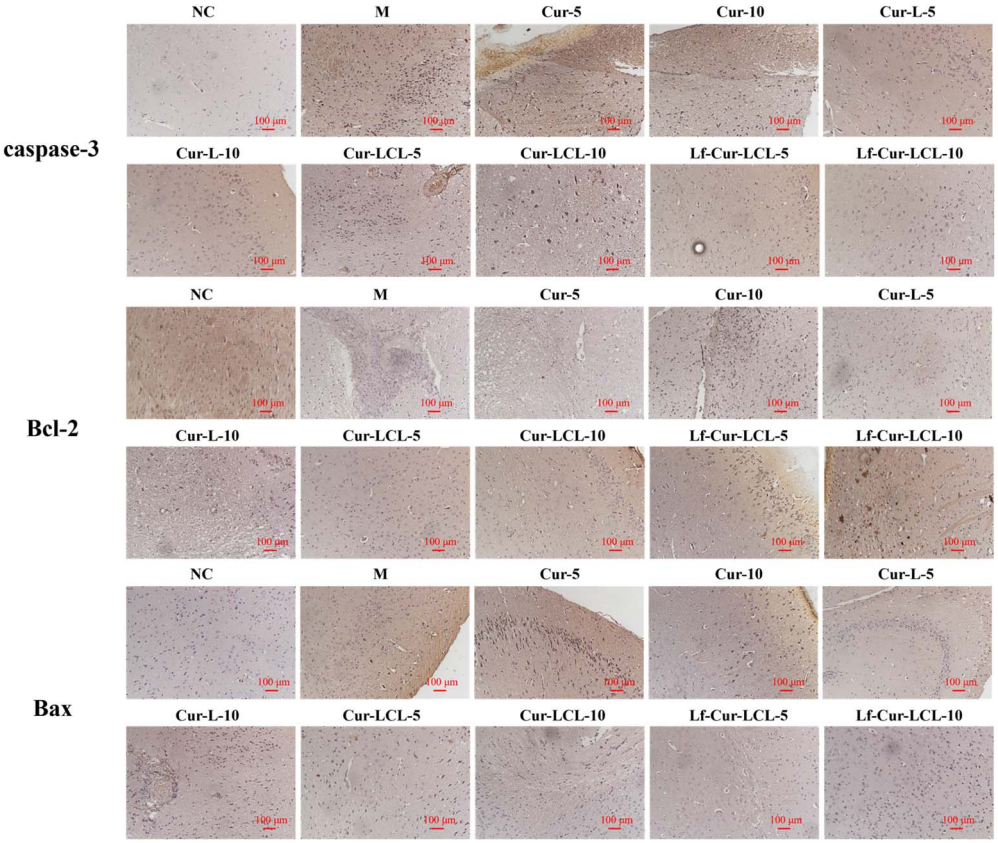

Fig. 9 Immunohistochemical (IHC) staining of brain tissue from different treatment groups. (20×, scale bar = 100 μm).

characterization of the binding affinity and thermodynamic properties of this interaction, helping to deepen our understanding of the structure–activity relationship in this delivery system.

4 Conclusion

In this study, three different Cur liposomes (Cur-L, Cur-LCL, and Lf-Cur-LCL) were prepared using the ethanol injection method. The quality of these liposomes was supported by enhancements in various parameters including PS, TEM, ZP, PDI, EE, DL, *in vitro* release, and cellular uptake of the nanopreparations. More importantly, the results demonstrate that these liposomes exhibit good quality and potential clinical application value. In addition, the three formulations showed significant effects in improving oxidative indicators and blood gas partial pressures, and reducing tissue damage in the liver, spleen, and kidneys of mice with CIH. Notably, the Lf-Cur-LCL formulation exhibited superior brain-targeting and therapeutic effects, thus indicating promising prospects for product development. By providing sustained release and enhancing tissue distribution, Lf-Cur-LCL offers a more effective therapeutic approach for brain-related conditions, including brain tumors and hypoxic brain injury.

The combination of Lf with long-circulating liposomes represents a significant advancement over traditional Cur formulations, unlocking new potential for targeted drug delivery in the treatment of neurological disorders. This development in Cur delivery systems holds considerable promise for clinical applications, particularly in overcoming the challenges associated with brain tumor therapy and other neurological diseases.

Conflicts of interest

There are no conflicts to declare.

Data availability

Data will be available upon request to the corresponding author.

Acknowledgements

This work was supported by People's Livelihood Scientific Research Special Medical and health project of Science and Technology Development Fund Institution in Shanghai Pudong New Area (PKJ2023-Y92), Pilot program personnel training project of People's Hospital in Shanghai Pudong New Area (PRYLH202401), the Health Technology Development Program of Nanjing (YKK22244), and the Medical Research Project of Jiangsu Health Commission (Z2021079).

© 2026 The Author(s). Published by the Royal Society of Chemistry

Open Access Article. Published on 07 November 2025. Downloaded on 1/9/2026 2:42:34 PM. This article is licensed under a Creative Commons Attribution-NonCommercial 3.0 Unported Licence.

References

1 G. Iannella, *et al.*, Obstructive Sleep Apnea Syndrome: From Symptoms to Treatment, *Int. Res. J. Publ. Environ. Health*, 2022, **19**(4), 2459.
2 S. Kumari, *et al.*, Obstructive Sleep Apnea in Metabolic Syndrome, *Ann. Afr. Med.*, 2024, **23**(4), 710–716.
3 K. Zasadzinska-Stempniak, H. Zajaczkiewicz and A. Kukwa, Prevalence of Obstructive Sleep Apnea in the Young Adult Population: A Systematic Review, *J. Clin. Med.*, 2024, **13**(5), 1386.
4 G. Labarca, *et al.*, Chronic intermittent hypoxia in obstructive sleep apnea: a narrative review from pathophysiological pathways to a precision clinical approach, *Sleep Breath.*, 2020, **24**, 751–760.
5 Y. Hao, *et al.*, Pulmonary Function Test and Obstructive Sleep Apnea Hypopnea Syndrome in Obese Adults: A Retrospective Study, *Int. J. Chronic Obstruct. Pulm. Dis.*, 2023, **18**, 1019–1030.
6 Z. Zhang, *et al.*, Prognostic effect of obstructive sleep apnea in acute coronary syndrome patients with heart failure, *Respir. Med.*, 2024, **234**, 107814.
7 M. Zhang, *et al.*, Advances in molecular pathology of obstructive sleep apnea, *Molecules*, 2022, **27**(23), 8422.
8 E. Díaz-García, *et al.*, Inflammasome Activation: A Keystone of Proinflammatory Response in Obstructive Sleep Apnea, *Am. J. Respir. Crit. Care Med.*, 2022, **205**(11), 1337–1348.
9 A. Jelska, *et al.*, The Role of Oxidative Stress and the Potential Therapeutic Benefits of Aronia melanocarpa Supplementation in Obstructive Sleep Apnea Syndrome: A Comprehensive Literature Review, *Antioxidants*, 2024, **13**(11), 16.
10 Y. Birling, Y. Wu and M. Rahimi, Chinese herbal medicine for obstructive sleep apnoea: a systematic review with meta-analysis, *Sleep Breath.*, 2025, **29**(1), 11.
11 F. A. Badria and A. A. Elgazar, Utilization of selected natural products as complementary therapeutic approach for Obstructive Sleep Apnea (OSA) management: a literature review, *Clin. Phytosci.*, 2024, **10**(1), 15.
12 M. Jabczyk, *et al.*, Curcumin in Metabolic Health and Disease, *Nutrients*, 2021, **13**(12), 4440.
13 J. Hu, *et al.*, Curcumin supplementation accelerates high-altitude acclimatization, prevents polycythemia and modulates gut microbiota in male Han population: a randomized controlled trial, *Front. Nutr.*, 2025, **12**, 1572376.
14 S. Moulin, *et al.*, Curcumin prevents chronic intermittent hypoxia-induced myocardial injury, *Ther. Adv. Chronic Dis.*, 2020, **11**, 2040622320922104.
15 B. Wang, *et al.*, Curcumin attenuates chronic intermittent hypoxia-induced brain injuries by inhibiting AQP4 and p38 MAPK pathway, *Respir. Physiol. Neurobiol.*, 2018, **255**, 50–57.
16 M. Erfanizadeh, *et al.*, Curcumin prevents neuronal loss and structural changes in the superior cervical (sympathetic) ganglion induced by chronic sleep deprivation, in the rat model, *Biol. Res.*, 2020, **53**(1), 15.
17 M. A. Elbaset, *et al.*, Curcumin nanoemulsion counteracts hepatic and cardiac complications associated with high-fat/high-fructose diet in rats, *J. Food Biochem.*, 2022, **46**, e14442.
18 L. F. Laurindo, *et al.*, Curcumin-Based Nanomedicines in the Treatment of Inflammatory and Immunomodulated Diseases: An Evidence-Based Comprehensive Review, *Pharmaceutics*, 2023, **15**(1), 229.
19 G. E. F. Abd-Ellatef, *et al.*, Curcumin-loaded solid lipid nanoparticles bypass P-glycoprotein mediated doxorubicin resistance in triple negative breast cancer cells, *Pharmaceutics*, 2020, **12**, 96.
20 M. M. El-Sherbiny, *et al.*, Fabrication and assessment of potent anticancer nanoconjugates from chitosan nanoparticles, curcumin, and eugenol, *Front. Bioeng. Biotechnol.*, 2022, **10**, 1030936.
21 L. Li, *et al.*, Curcumin-carbon dots suppress periodontitis via regulating METTL3/IRE1α signaling, *Crit. Rev. Eukaryot. Gene Expr.*, 2025, **35**(1), 25–35.
22 G. A. Tawfeek, *et al.*, Curcumin Nanofiber PCL/PLGA/Collagen Enhanced the Therapeutic Efficacy of Mesenchymal Stem Cells against Liver Fibrosis in Animal Model and Prevented its Recurrence, *Nanotheranostics*, 2023, **7**(3), 299–315.
23 J. Chen, *et al.*, Curcumin-loaded hydrogels promote skin wound healing, *Soft Matter*, 2025, **21**(37), 7184–7203.
24 H. K. Jahromi, *et al.*, Enhanced sciatic nerve regeneration by poly-L-lactic acid/multi-wall carbon nanotube neural guidance conduit containing Schwann cells and curcumin encapsulated chitosan nanoparticles in rat, *Mater. Sci. Eng., C*, 2020, **109**, 110564.
25 K. Möller, B. Macaulay and T. Bein, Curcumin encapsulated in crosslinked cyclodextrin nanoparticles enables immediate inhibition of cell growth and efficient killing of cancer cells, *Nanomaterials*, 2021, **11**, 489.
26 C. H. Liu, *et al.*, Encapsulating curcumin in ethylene diamine-β-cyclodextrin nanoparticle improves topical cornea delivery, *Colloids Surf. B Biointerfaces*, 2020, **186**, 110726.
27 X. Q. Wei and K. Ba, Construction a Long-Circulating Delivery System of Liposomal Curcumin by Coating Albumin, *ACS Omega*, 2020, **5**, 16502–16509.
28 N. Qiu, *et al.*, A review of stimuli-responsive polymeric micelles for tumor-targeted delivery of curcumin, *Drug Dev. Ind. Pharm.*, 2021, **47**(6), 839–856.
29 X. Liu, *et al.*, Curcumin and its novel formulations for diabetes mellitus and its complications: a review, *Food Funct.*, 2025, **16**(18), 6965–6999.
30 Y. Tang, *et al.*, Overcoming the reticuloendothelial system barrier to drug delivery with a "don't-eat-us" strategy, *ACS Nano*, 2019, **13**(11), 13015–13026.
31 Y. Shi, *et al.*, Nano-formulations in disease therapy: designs, advances, challenges, and future directions, *J. Nanobiotechnol.*, 2025, **23**(1), 396.
32 V. De Leo, *et al.*, Liposomes containing nanoparticles: preparation and applications, *Colloids Surf B Biointerfaces*, 2022, **218**, 112737.

Open Access Article. Published on 07 November 2025. Downloaded on 1/9/2026 2:42:34 PM. This article is licensed under a Creative Commons Attribution-NonCommercial 3.0 Unported Licence.

33 L. E. Waggoner, *et al.*, Analysis of PEG-lipid anchor length on lipid nanoparticle pharmacokinetics and activity in a mouse model of traumatic brain injury, *Biomater. Sci.*, 2023, **11**(12), 4238–4253.
34 S. V. Morse, *et al.*, Liposome delivery to the brain with rapid short-pulses of focused ultrasound and microbubbles, *J. Contr. Release*, 2022, **341**, 605–615.
35 Y.-Q. Li and C. Guo, A review on lactoferrin and central nervous system diseases, *Cells*, 2021, **10**(7), 1810.
36 S. Wang, *et al.*, Molecular Characterization and Expression of Lactoferrin Receptor (LfR) in Different Regions of the Brain Responding to Lactoferrin Intervention, *Mol. Neurobiol.*, 2025, **62**(3), 2857–2871.
37 A. O. Elzoghby, *et al.*, Lactoferrin, a multi-functional glycoprotein: Active therapeutic, drug nanocarrier & targeting ligand, *Biomaterials*, 2020, **263**, 120355.
38 F. Guzmán-Mejía, *et al.*, Lactoferrin as a Component of Pharmaceutical Preparations: An Experimental Focus, *Pharmaceuticals*, 2023, **16**, 214.
39 H. P. Nijhawan, *et al.*, PEGylated pH-Responsive Liposomes for Enhancing the Intracellular Uptake and Cytotoxicity of Paclitaxel in MCF-7 Breast Cancer Cells, *AAPS PharmSciTech*, 2024, **25**(7), 216.
40 M. A. De Luca, *et al.*, Lactoferrin- and antitransferrin-modified liposomes for brain targeting of the NK3 receptor agonist senktide: Preparation and in vivo evaluation, *Int. J. Pharm.*, 2015, **479**(1), 1129–1137.
41 A. Wu, *et al.*, In Vitro and In Vivo Evaluation of Lactoferrin-Modified Liposomal Etomidate with Enhanced Brain-Targeting Effect for General Anesthesia, *Pharmaceutics*, 2024, **16**, 805.
42 Y. Yang, *et al.*, Modified Ce/Zr-MOF Nanoparticles Loaded with Curcumin for Alzheimer's Disease via Multifunctional Modulation, *Int. J. Nanomed.*, 2024, **19**, 9943–9959.
43 G. Du and X. Sun, Ethanol Injection Method for Liposome Preparation, *Methods Mol. Biol.*, 2023, **2622**, 65–70.
44 J. Liu, *et al.*, Preparation, characterization, pharmacokinetics, and antirenal injury activity studies of Licochalcone A-loaded liposomes, *J. Food Biochem.*, 2022, **46**(1), e14007.
45 T. M. Pereira, *et al.*, Rapid and Versatile Biosensing of Liposome Encapsulation Efficiency Using Electrical Conductivity Sensor, *Biosensors (Basel).*, 2023, **13**(9), 878.
46 P. Kundu, *et al.*, Delivery of Dual Drug Loaded Lipid Based Nanoparticles across the Blood–Brain Barrier Impart Enhanced Neuroprotection in a Rotenone Induced Mouse Model of Parkinson's Disease, *ACS Chem. Neurosci.*, 2016, **7**(12), 1658–1670.
47 F. Guo, *et al.*, Matrix metalloprotein-triggered, cell penetrating peptide-modified star-shaped nanoparticles for tumor targeting and cancer therapy, *J. Nanobiotechnol.*, 2020, **18**, 48.
48 P. Xu, *et al.*, TAK1 mediates neuronal pyroptosis in early brain injury after subarachnoid hemorrhage, *J. Neuroinflammation*, 2021, **18**(1), 188.
49 L. Xu, *et al.*, Chronic Intermittent Hypoxia-Induced Aberrant Neural Activities in the Hippocampus of Male Rats Revealed by Long-Term in vivo Recording, *Front. Cell. Neurosci.*, 2022, **15**, 784045.
50 J. Górnicka, *et al.*, Methods to Improve the Solubility of Curcumin from Turmeric, *Life (Basel)*, 2023, **13**(1), 207.
51 R. Khursheed, *et al.*, Development and Validation of RP-HPLC Method for Simultaneous Determination of Curcumin and Quercetin in Extracts, Marketed Formulations, and Self-Nanoemulsifying Drug Delivery System, *J. Pharm. Res.*, 2021, **13**(10), 43–52.
52 G. Yenduri, *et al.*, Impact of critical process parameters and critical material attributes on the critical quality attributes of liposomal formulations prepared using continuous processing, *Int. J. Pharm.*, 2022, **619**, 121700.
53 B. Hoseini, *et al.*, Optimizing nanoliposomal formulations: Assessing factors affecting entrapment efficiency of curcumin-loaded liposomes using machine learning, *Int. J. Pharm.*, 2023, **646**, 123414.
54 M. I. Teixeira, *et al.*, Riluzole-loaded lipid nanoparticles for brain delivery: Preparation, optimization and characterization, *J. Mol. Liq.*, 2023, **388**, 17.
55 B. Hoseini, *et al.*, Application of ensemble machine learning approach to assess the factors affecting size and polydispersity index of liposomal nanoparticles, *Sci. Rep.*, 2023, **13**, 18012.
56 G. Midekessa, *et al.*, Zeta Potential of Extracellular Vesicles: Toward Understanding the Attributes that Determine Colloidal Stability, *ACS Omega*, 2020, **5**(27), 16701–16710.
57 Y. Zhang, *et al.*, Sodium dodecyl sulfate improved stability and transdermal delivery of salidroside-encapsulated niosomes via effects on zeta potential, *Int. J. Pharm.*, 2020, **580**, e119183.
58 S. Kopanchuk, *et al.*, Zeta Potential of Extracellular Vesicles: Toward Understanding the Attributes that Determine Colloidal Stability, *ACS Omega*, 2020, **5**(27), 16701–16710.
59 J. Liu, *et al.*, Preparation, characterization, pharmacokinetics, and antirenal injury activity studies of Licochalcone A-loaded liposomes, *J. Food Biochem.*, 2022, **46**(1), e14007.
60 C. Yu, *et al.*, Co-Encapsulation of Curcumin and Diosmetin in Nanoparticles Formed by Plant-Food-Protein Interaction Using a pH-Driven Method, *Foods*, 2023, **12**, 2861.
61 W. Zhang, *et al.*, Effects of morphology and size of nanoscale drug carriers on cellular uptake and internalization process: a review, *RSC Adv.*, 2023, **13**(1), 80–114.
62 K. Tai, *et al.*, Stability and release performance of curcumin-loaded liposomes with varying content of hydrogenated phospholipids, *Food Chem.*, 2020, **326**, 126973.
63 V. Campani, *et al.*, Skin permeation and thermodynamic features of curcumin-loaded liposomes, *J. Mater. Sci.: Mater. Med.*, 2020, **31**, 18.
64 A. L. Luss, *et al.*, Toxicity Evaluation and Controlled-Release of Curcumin-Loaded Amphiphilic Poly-N-vinylpyrrolidone Nanoparticles: In Vitro and In Vivo Models, *Pharmaceutics*, 2024, **16**(1), 16.
65 Z. Liu, J. D. Smart and A. S. Pannala, Recent developments in formulation design for improving oral bioavailability of

© 2026 The Author(s). Published by the Royal Society of Chemistry

Open Access Article. Published on 07 November 2025. Downloaded on 1/9/2026 2:42:34 PM.
This article is licensed under a Creative Commons Attribution-NonCommercial 3.0 Unported Licence.

curcumin: A review, *J. Drug Delivery Sci. Technol.*, 2020, **60**, 102082.
66 J. W. Song, *et al.*, Nano-Liposomes Double Loaded with Curcumin and Tetrandrine: Preparation, Characterization, Hepatotoxicity and Anti-Tumor Effects, *Int. J. Mol. Sci.*, 2022, **23**(12), 13.
67 H. W. Chen, *et al.*, Improvement in Curcumin's Stability and Release by Formulation in Flexible Nano-Liposomes, *Nanomaterials (Basel)*, 2024, **14**(22), 1836.
68 V. Nagati, *et al. Chapter 4 - Stability of Therapeutic Nano-Drugs during Storage and Transportation as Well as after Ingestion in the Human body.Advances in Nanotechnology-Based Drug Delivery Systems*, Nanotech Biomed, 2022, P.83–102.
69 M. Agrawal, *et al.*, Recent advancements in liposomes targeting strategies to cross blood–brain barrier (BBB) for the treatment of Alzheimer's disease, *J. Contr. Release*, 2017, **260**, 61–77.
70 F. Zahednezhad, *et al.*, Liposome and immune system interplay: Challenges and potentials, *J. Controlled Release*, 2019, **305**, 194–209.
71 P. Prathipati, A Retrospective Analysis for Different Routes of Administration in Mice-Percutaneous Retro-Orbital, Jugular Catheter, Tail Vein and Femoral Cut Down Injections, *JBM*, 2020, **8**(9), 131–141.
72 K. Godbout and J. P. Tremblay, Delivery of RNAs to Specific Organs by Lipid Nanoparticles for Gene Therapy, *Pharmaceutics*, 2022, **14**(10), 2129.
73 P. V. Turner, *et al.*, Administration of substances to laboratory animals: routes of administration and factors to consider, *J. Am. Assoc. Lab. Anim. Sci.*, 2011, **50**(5), 600–613.
74 C. Conesa, *et al.*, The Role of Lactoferrin in Intestinal Health, *Pharmaceutics*, 2023, **15**, 1569.
75 F. Pognan, *et al.*, The evolving role of investigative toxicology in the pharmaceutical industry, *Nat. Rev. Drug Discov.*, 2023, **22**, 317–335.
76 M. I. Teixeira, *et al.*, Surface-modified lipid nanocarriers for crossing the blood–brain barrier (BBB): A current overview of active targeting in brain diseases, *Colloids Surf. B Biointerfaces*, 2023, **221**, 112999.
77 S. Mittal, *et al.*, Ligand conjugated targeted nanotherapeutics for treatment of neurological disorders, *Curr. Pharm. Des.*, 2020, **26**(19), 2291–2305.
78 L. Han and C. Jiang, Evolution of blood–brain barrier in brain diseases and related systemic nanoscale brain-targeting drug delivery strategies, *Acta Pharm. Sin. B*, 2021, **11**(8), 2306–2325.
79 J. Liu, *et al. Delivery of Biomimetic Liposomes via Meningeal Lymphatic Vessels Route for Targeted Therapy of Parkinson's Disease*, Research (Wash D C), 2023, 6, p. 0030.
80 M. Gomes, *et al.*, Advancing Brain Targeting: Cost-Effective Surface-Modified Nanoparticles for Faster Market Entry, *Pharmaceutics*, 2025, **17**(5), 661.
81 F. Juhairiyah, *et al.*, Understanding Drug Delivery to the Brain Using Liposome-Based Strategies: Studies that Provide Mechanistic Insights Are Essential, *AAPS J.*, 2021, **23**(6), 114.
82 H. Truby, *et al.*, A 12-month weight loss intervention in adults with obstructive sleep apnoea: is timing important? A step wedge randomised trial, *Eur. J. Clin. Nutr.*, 2022, **76**(12), 1762–1769.
83 P. K. Schweitzer, *et al.*, Solriamfetol for Excessive Sleepiness in Obstructive Sleep Apnea (TONES 3). A Randomized Controlled Trial, *Am. J. Respir. Crit. Care Med.*, 2019, **199**(11), 1421–1431.
84 A. Malhotra, *et al.*, Tirzepatide for the Treatment of Obstructive Sleep Apnea and Obesity, *N. Engl. J. Med.*, 2024, **391**(13), 1193–1205.
85 S. Luu, *et al.*, Pharmacotherapy for obstructive sleep apnea: a critical review of randomized placebo-controlled trials, *Sleep Med. Rev.*, 2025, **84**, 102169.